Sudden Stratospheric Warmings in the Northern Hemisphere Observed With IASI

Marie Bouillon, Sarah Safieddine, Cathy Clerbaux

JGR Atmospheres

RESEARCH ARTICLE
10.1029/2023JD038692

Sudden Stratospheric Warmings in the Northern Hemisphere Observed With IASI

Marie Bouillon[1], **Sarah Safieddine**[1], **and Cathy Clerbaux**[1,2]

[1]LATMOS/IPSL, Sorbonne Université, UVSQ, CNRS, Paris, France, [2]Université libre de Bruxelles (ULB), Spectroscopy, Quantum Chemistry and Atmospheric Remote Sensing (SQUARES), Brussels, Belgium

Key Points:

- Sudden Stratospheric Warmings impact temperature at all altitudes and can cause cold air outbreaks at midlatitudes
- Ozone springtime concentrations are strongly linked to the occurrence of major Sudden Stratospheric Warmings
- The Infrared Atmospheric Sounding Interferometers are efficient tools to study temperature and ozone during Sudden Stratospheric Warmings

Supporting Information:

Supporting Information may be found in the online version of this article.

Correspondence to:

M. Bouillon,
marie.bouillon@latmos.ipsl.fr

Citation:

Bouillon, M., Safieddine, S., & Clerbaux, C. (2023). Sudden stratospheric warmings in the Northern Hemisphere observed with IASI. *Journal of Geophysical Research: Atmospheres*, *128*, e2023JD038692. https://doi.org/10.1029/2023JD038692

Received 10 FEB 2023
Accepted 15 AUG 2023

Abstract Sudden Stratospheric Warming events (SSW) are extreme phenomena during which stratospheric temperature can increase by tens of degrees in a few days. They are due to the propagation and breaking of the planetary waves, leading to a perturbation of the polar vortex. SSWs also influence polar ozone concentrations and midlatitude weather. The Infrared Atmospheric Sounding Interferometers (IASI) monitor atmospheric composition and temperature globally since 2007, and they are ideal to observe the changes of temperature and ozone during SSWs. Since the launch of the first IASI, there have been several SSWs in the Northern Hemisphere, including eight major events that are investigated in this study. We find that during major SSWs, the temperature anomaly propagates from 10 hPa to the lower stratosphere and the maximum anomaly at 200 hPa is correlated to the maximum anomaly at 10 hPa. During these events, negative anomalies of temperature in Europe and Russia and positive anomalies in Canada and Greenland are often observed at 750 hPa. The cold air outbreaks that usually follow major SSWs are responsible for anomalies of −15 K. Finally, we look at the evolution of the total ozone column following major events. Major SSWs lead to higher springtime ozone concentrations and the ozone anomaly in March is correlated to the duration of the positive temperature anomaly at 10 hPa. These results show the potential of the IASI mission and its successors, IASI-New Generation, for the study of SSWs and their effects on weather and atmospheric composition.

Plain Language Summary Sudden Stratospheric Warming (SSW) events are extreme events during which stratospheric temperature can increase by tens of degrees in a few days. Although they happen in the stratosphere, they have effects on midlatitude weather and ozone concentrations. With observation from the Infrared Atmospheric Sounding Interferometers, we find that temperature anomalies associated with SSW propagate from the upper to the lower stratosphere. They are also responsible for cold air outbreaks in North America and Europe. Finally, we find that SSWs lead to larger ozone concentrations in the spring.

1. Introduction

Sudden Stratospheric Warmings (SSW) are one of the most impressive phenomena happening in the atmosphere. In typical winter conditions, as insolation decreases and the meridional temperature gradient increases, a polar stratospheric vortex forms over the poles, with winds blowing westerly. When an abnormally large tropospheric planetary wave propagates vertically, stratospheric circulation (Baldwin et al., 2021; Butler et al., 2015; Schoeberl, 1978) is perturbed. As a result, stratospheric polar temperature can increase by several tens of degrees over a few days, and westerly winds slow down or even reverse to easterlies (Butler et al., 2017; Maury et al., 2016) and it can cause the polar vortex to be displaced or to break down. SSWs have a strong impact on the winter global circulation and they are the main source of intraseasonal and interannual variability in the extratropical stratosphere (De la Cámara, Abalos, Hitchcock, Calvo, & Garcia, 2018).

SSWs are usually categorized as minor or major events (Butler et al., 2017). Major SSWs are characterized by the inversion of zonal winds at 10 hPa and 60°N (or 60°S in the Southern Hemisphere) and an inversion of the North-South temperature gradient at 10 hPa and 60°N (60°S). During minor SSWs, there is an inversion of the temperature gradient but the zonal winds only decelerate and do not reverse to easterlies (Butler et al., 2017). For two major events to be considered as distinct SSWs, there has to be at least 20 days of westerly zonal winds in between. In the Northern Hemisphere, major SSWs happen on average 6 times per decade (Charlton & Polvani, 2007). They are much less frequent in the Southern Hemisphere, as the amplitude of planetary waves is smaller (Van Loon et al., 1973) and the polar vortex more stable due to the presence of the Antarctic continent.

Although they occur due to the propagation of planetary waves to the polar stratosphere, SSWs are known to cause surface temperature anomalies at midlatitudes (Lu et al., 2021a; Rao et al., 2020, 2021): as the stratospheric cold air propagates downwards to the troposphere, it can disturb the jet stream and create tropospheric blockings over the North Atlantic and Scandinavia which leads to cold anomalies over North America and Eurasia, and warm anomalies over Canada and Greenland (Baldwin et al.,. 2021; Butler et al., 2015; Thompson et al., 2002). Because of their impact on tropospheric weather, SSWs may also influence atmospheric pollution (Lu et al., 2021b, 2022).

SSWs also have an impact on observed ozone concentrations. First, when the SSW occurs, ozone concentrations increase as transport and mixing are enhanced during these evens (Bahramvash Shams et al., 2022; De la Cámara, Abalos, Hitchcock, Calvo, & Garcia, 2018). Furthermore, SSWs have a strong impact on ozone depletion during spring. In typical winter conditions, extremely cold stratospheric temperature lead to the condensation of water vapor and nitric acid into polar stratospheric clouds (PSC). These clouds contain ideal conditions to transform chlorine and bromine reservoirs into ozone depleting radicals, that are activated when sunlight comes back to the poles, leading to ozone depletion in the spring. The abnormally large stratospheric temperatures observed during SSWs significantly hinder the formation of PSCs, thus altering the whole ozone depletion process (De la Cámara, Abalos, Hitchcock, Calvo, & Garcia, 2018; Manney et al., 2011; Manney & Lawrence, 2016; Safieddine, Bouillon, et al., 2020; Salmi et al., 2011).

The Infrared Atmospheric Sounding Interferometers (IASI) onboard the Metop satellites are ideal instruments to observe SSWs and their effects, as daily and global atmospheric temperatures and ozone concentrations can be retrieved simultaneously.

In this study, we use temperature and ozone from IASI to analyze eight major SSWs that happened in the Northern Hemisphere since the winter of 2007–2008. The data sets used in this study are presented in Section 2. Section 3.1 describes the evolution of stratospheric temperature during SSWs, Section 3.2 the effects on tropospheric weather at midlatitudes and Section 3.3 the ozone concentrations following SSWs. We conclude by discussing the limits and perspectives of our work in Section 4.

2. Data and Methods

2.1. IASI Atmospheric Temperatures and Ozone Total Columns

The Infrared Atmospheric Sounding Interferometers (IASI), launched in 2006 (IASI-A), 2012 (IASI-B) and 2018 (IASI-C), measure radiance spectra in the thermal infrared, between 645 and 2,760 cm^{-1}, from which we can retrieve surface and atmospheric temperatures (Bouillon et al., 2022; Safieddine, Parracho, et al., 2020) and trace gas concentrations (Clarisse et al., 2011; Clerbaux et al., 2009). Each of the IASI instrument covers the whole globe twice a day with an ability to scan across track, providing a good spatial coverage. Since the IASI mission is planned to fly for at least 18 years, long and stable times series of atmospheric temperature and composition can be retrieved from their observations.

The temperature data used in this work was calculated from the homogeneous IASI radiance record released by the EUropean organisation for the exploitation of METeorological SATellites (EUMETSAT) in 2018 (EUMETSAT, 2018). Temperatures were computed at 11 pressure levels (2, 7, 10, 20, 30, 70, 100, 200, 400, 550, and 750 hPa) using an artificial neural network trained with IASI radiances at ∼700 and 2,200 cm^{-1} as input and ERA5 temperatures as output. Validation of this product with radio sounding observations and with ERA5 shows that it is suitable for the analysis of temperature distribution and trends (Bouillon et al., 2022).

The daily temperature anomalies were computed as the temperature each day minus the all the other years average temperature of the same day, for each pressure level. The meridional temperature gradient was computed with this temperature data record, using the average zonal temperature between 59° and 60° minus the average zonal temperature between 60° and 61°.

In this study, we also used total ozone columns colocated with the temperature data. These are retrieved from the 860–900 cm^{-1} and 1,025–1,075 cm^{-1} ozone absorption bands with the Fast Optimal Retrievals on Layers for IASI (FORLI) algorithm (Hurtmans et al., 2012). Total ozone columns from IASI have been validated (Boynard et al., 2009, 2016, 2018) and widely used to monitor polar ozone and its evolution (Clerbaux et al., 2009; Safieddine, Bouillon, et al., 2020; Scannell et al., 2012; Wespes et al., 2016). The IASI sensitivity to the ozone

profile is maximal in the middle troposphere, the upper troposphere and lower stratosphere (Boynard et al., 2009). The daily ozone anomalies were computed using the same method as for the temperature anomalies.

2.2. ERA5 Reanalysis of Zonal Winds

We also use the hourly zonal wind data at 10 hPa and 60°N from ERA5, the latest reanalysis data set from the European Centre for Medium-range Weather Forecasts (ECMWF). ERA5 is based on both in-situ and remote sensing observations assimilated into ECMWF's Integrated Forecast System (IFS), and it provides atmospheric, oceanic and land variables (Hersbach et al., 2020). ERA5 hourly data is given on a 0.25° × 0.25° latitude-longitude grid.

3. Results

In the following, we use temperature grids at different altitudes (10, 200, and 750 hPa) and ozone total columns daily grids from IASI, and the corresponding ERA5 zonal winds at 10 hPa, over all the winters covered in the IASI period. In order to extend the discussion to understand the short time effect of SSWs on the troposphere, "winter" in this study refers to the period from December 1st to March 31st. For the rest of this study, we use the SSW definition from Butler et al., 2017: minor SSWs are defined by the reversal of the temperature gradient at 60°N and 10 hPa and major SSWs are defined by the reversal of the temperature gradient and the reversal of zonal wind at 60° and 10 hPa.

3.1. Evolution of Stratospheric Temperature During SSWs

Contrary to minor SSWs that happen at least once a year, major SSWs are much less frequent: only eight major SSWs happened since 2007–2008. Figure 1 shows the evolution of the temperature gradient (from IASI, computed with the average zonal temperature between 60° and 61° minus the average zonal temperature between 59° and 60°) and zonal winds (from ERA5) at 10 hPa and 60°N during the eight winters during which a major SSW happened, since the launch of the first IASI. The dates of these major SSWs (date of the zonal wind inversion) are listed in Table 1. The maximum anomalies for temperature and ozone in Table 1 are defined as the largest daily anomaly of the average temperature between 60°N and 90°N, of all the days between the 1st of December and the 31st of March. The results listed in this table will be discussed more in detail hereafter.

Figure 1 shows that during the winters of 2008–2009, 2012–2013, 2017–2018, and 2020–2021, the inversions of the temperature gradient and zonal winds happened almost simultaneously (inversion of the temperature gradient occurred four days, one day, one day, and three days before the inversion of zonal wind, respectively).

The maximum anomalies for temperature and ozone in Table 1 are defined as the largest daily anomaly of the average temperature between 60°N and 90°N, of all the days between the 1st of December and the 31st of March. The results listed in this table will be discussed more in detail hereafter. The type of SSW event listed in Table 1 refers to the mode of the vortex movement during the event, which can be either a displacement or a split. To illustrate this, Figure 2 shows a time lapse of the temperature at 10 hPa during each of the events listed in Table 1 to illustrate the vortex split or displacement.

The major SSWs of February 2008, January 2010, March 2016, and December 2018 were associated to a displacement of the polar vortex. During these four events, we see that the vortex is pushed toward the Europe-North Atlantic-North America region by warm air coming from Eastern Asia. On the other hand, the SSWs of January 2009, January 2013, February 2018, and January 2021 were associated to a vortex split. As Figure 2 shows, these four events, the vortex was split by two air masses coming from Eastern Asia and Greenland.

Figure 3 shows the average daily temperature anomaly between 60°N and 90°N from December 1st to March 31st. We see that the dates of positive temperature anomalies match the dates of the temperature gradient inversions. We note how during the winter of 2007–2008, the temperature anomaly above 30 hPa is positive at three different dates, matching the dates of the temperature gradient inversions, before a fourth increase in mid-February, matching the date of the zonal wind inversion. This last increase went lower into the stratosphere (+10 K down to 100 hPa and +5 K down to 200 hPa) and lasted several weeks.

The winter of 2015–2016 also had a mild positive anomaly at the time of the gradient inversion followed by a stronger one at the beginning of March, starting with the zonal wind inversion, that went down as low as 300 hPa.

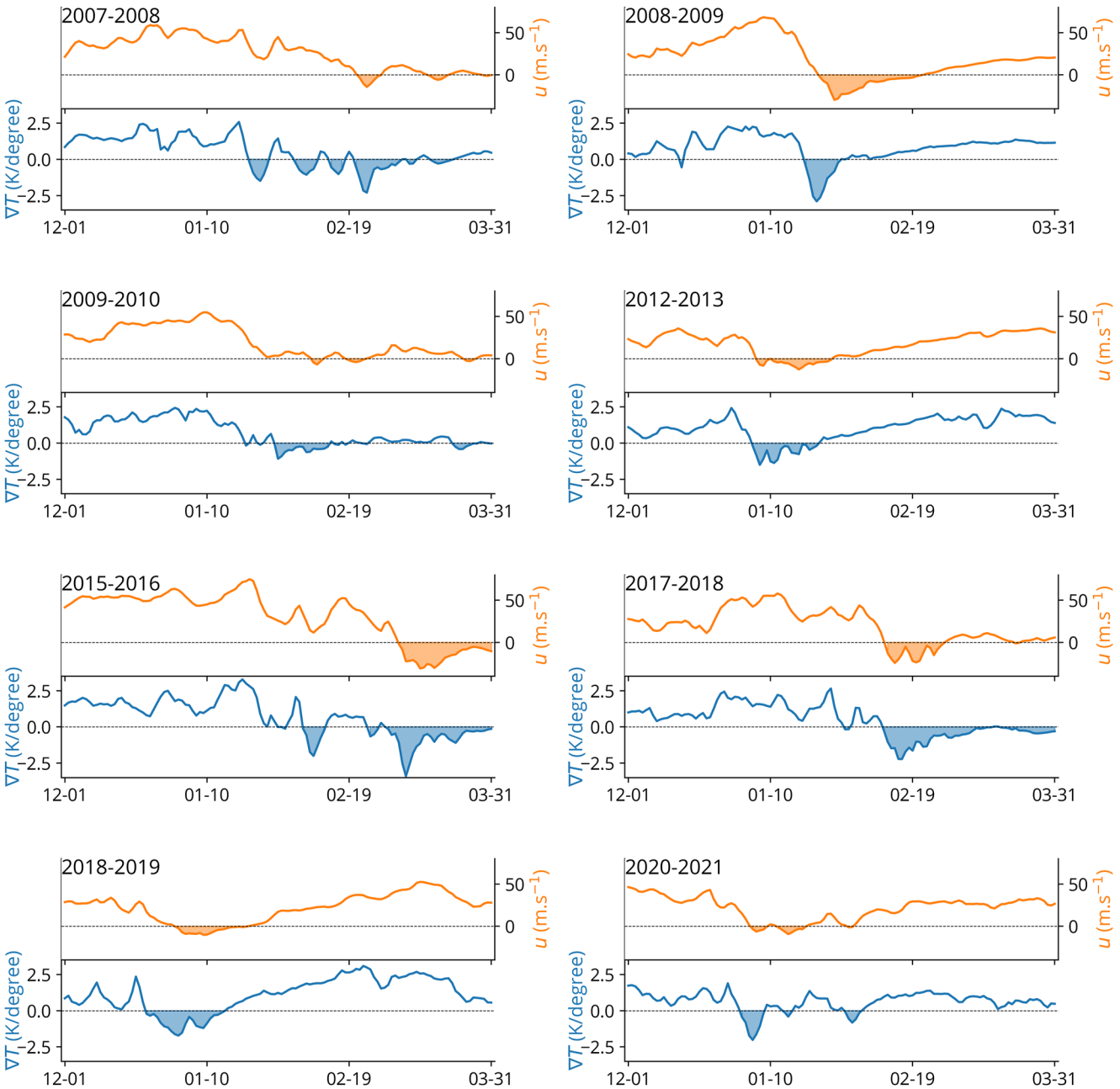

Figure 1. Zonal wind (orange, from ERA5) and North-South temperature gradient (blue, from IASI) at 60°N and 10 hPa between December 1st and March 31st.

In 2008–2009, there was a single but very intense temperature positive anomaly in late January. It propagated down to 300 hPa and lasted until mid-March. A similar scenario happened in 2018–2019, with a very strong positive anomaly of temperature starting in late December at the time of the temperature gradient inversion, and lasting until early February. The winters of 2009–2010, 2012–2013, 2017–2018, and 2020–2021 had a single and relatively strong positive anomaly of temperature. We see that during major SSWs, the temperature anomaly linked to the zonal wind inversion propagates lower into the stratosphere, reaching the tropopause at ∼300 hPa, and lasts a few weeks after the beginning of the SSW, which is not the case for minor SSWs. This is consistent with the results of Baldwin and Dunkerton (2001), and Hitchcock and Simpson (2014).

To illustrate and quantify the downward propagation of the anomaly, Figure 4 shows the maximum temperature anomaly at 10 and 200 hPa during the eight studied winters and the average anomaly in the 10 (10 hPa) or 30

Table 1
The Eight Major SSWs of [2008–2021]: Dates of the Zonal Wind and Temperature Gradient Inversion, Maximum Temperature Anomalies at 10 hPa and 200 hPa and Their Dates, and the Maximum Ozone Anomaly for Each of the Major SSWs

Date of first T gradient inversion	Date of zonal wind inversion	Type of event	Max T anomaly at 10 hPa	Date of max T anomaly at 10 hPa	Max T anomaly at 200 hPa	Date of max T anomaly at 200 hPa	Maximum O_3 anomaly
2008 01 22	2008 02 22	Displacement	30.1 K	2008 02 23	6.2 K	2008 03 30	64.0 DU
2009 01 20	2009 01 24	Split	37.6 K	2009 01 23	11.3 K	2009 02 25	117.1 DU
2010 01 29	2010 02 09	Displacement	17.4 K	2010 12 30	8.1 K	2010 02 12	74.7 DU
2013 01 05	2013 01 13	Split	22.4 K	2013 01 11	8.7 K	2013 01 18	79.4 DU
2016 02 05	2016 03 05	Displacement	33.1 K	2016 03 06	6.5 K	2016 03 15	68.5 DU
2018 02 11	2018 02 12	Split	29.1 K	2018 02 17	7.1 K	2018 03 19	74.3 DU
2018 12 24	2019 01 01	Displacement	36.1 K	2018 12 28	8.4 K	2019 01 13	117.0 DU
2021 01 02	2021 01 05	Split	29.1 K	2021 01 04	7.1 K	2021 01 22	73.9 DU

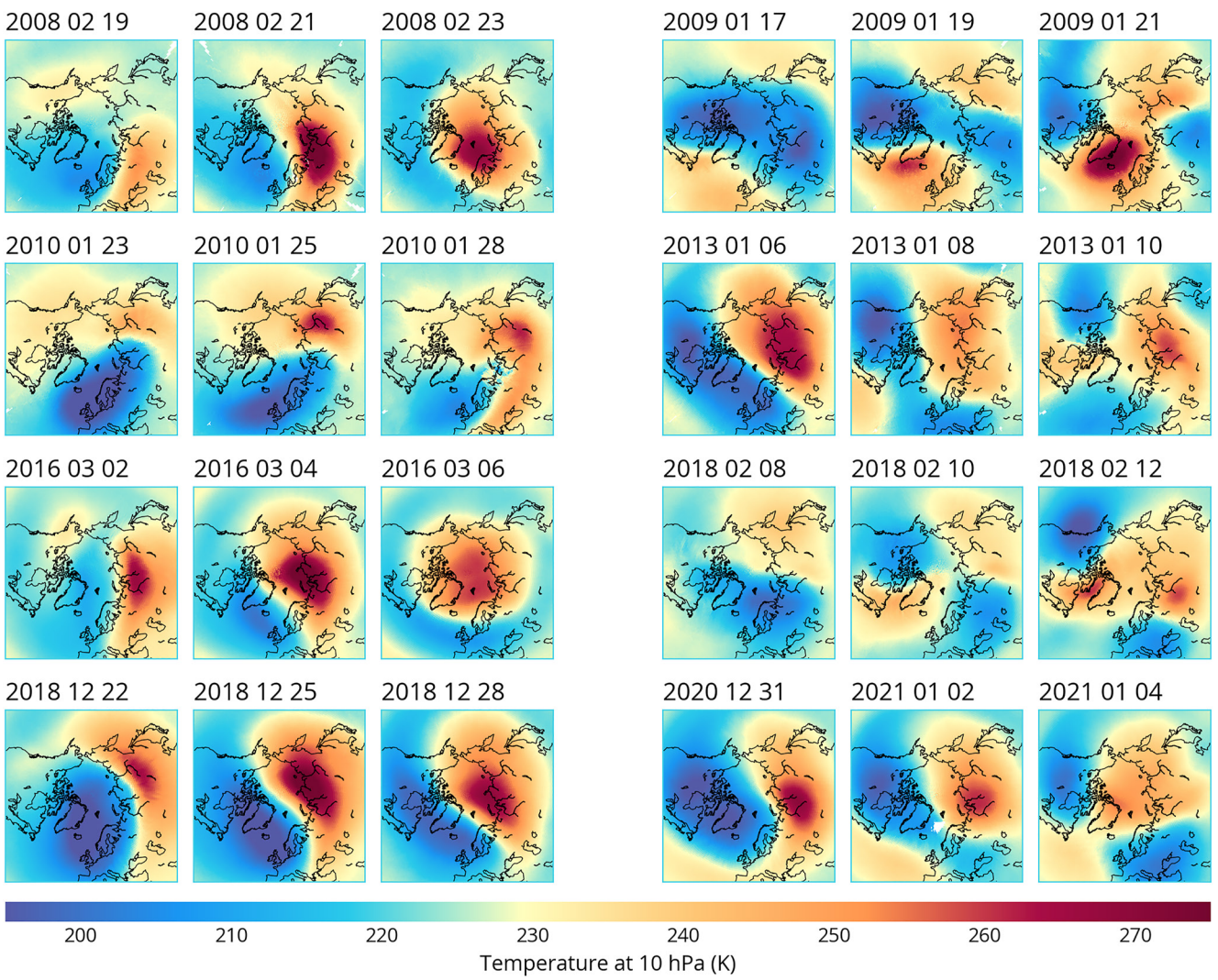

Figure 2. Temperature at 10 hPa showing the displacement or split of the polar vortex during the eight major SSWs observed by IASI.

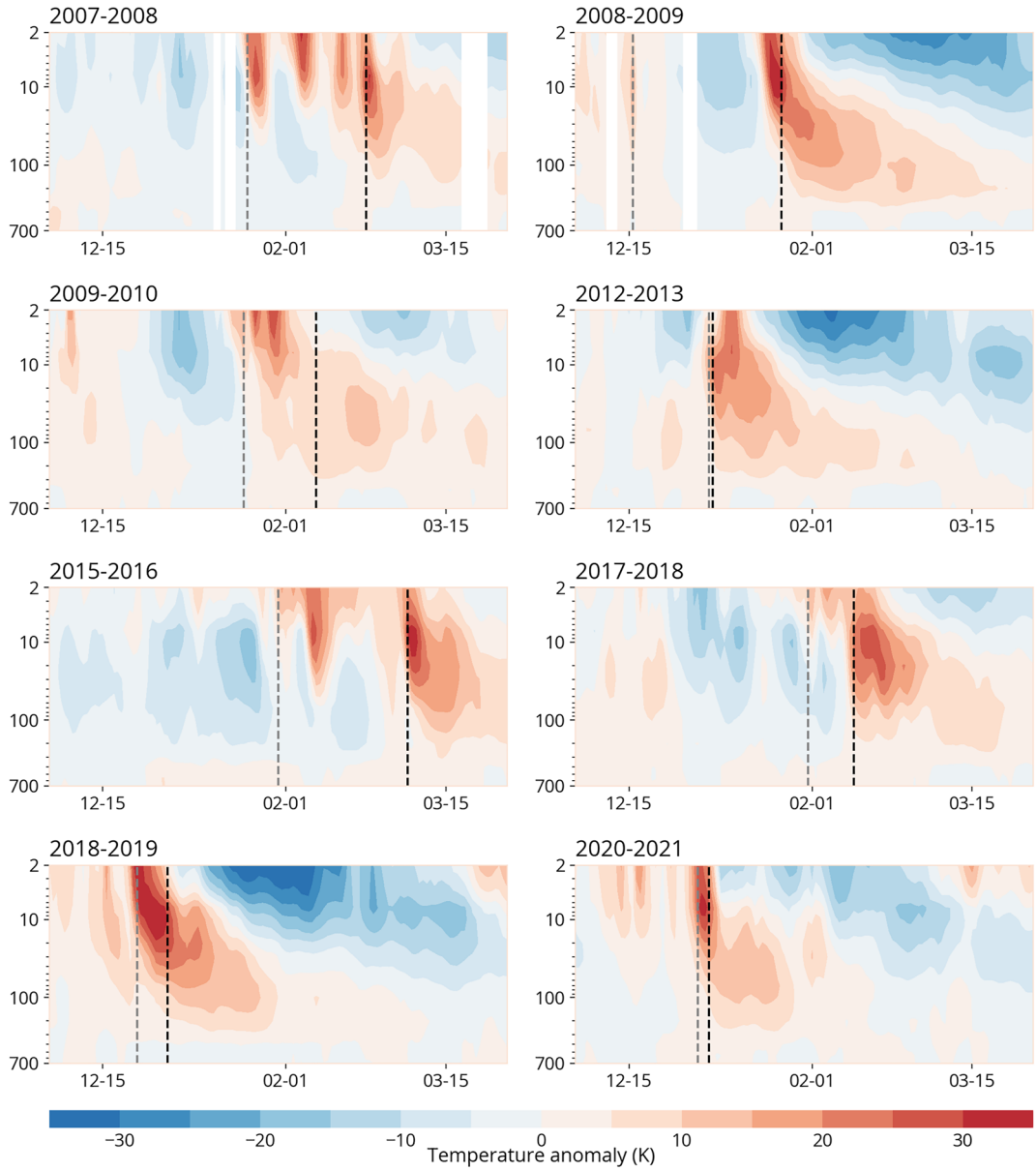

Figure 3. Temperature anomaly between 60°N and 90°N between December 1st and March 31st of each year with a major SSW. The black dashed lines represent the dates of the zonal wind inversion, and the gray lines represent the dates of the first temperature gradient inversion.

(200 hPa) days following the zonal wind inversion, as well as the relationship between maximum anomalies at 10 and 200 hPa, and the relationship between the dates at which they were reached.

The average anomaly during the 10 days following the zonal wind inversion (Figure 4a) is usually between 10 and 25 K, with the average anomalies of 2012–2013, 2015–2016, 2017, 2018, and 2018–2019 exceeding 20 K (20.6, 22.5, 24.6, and 20.2 K respectively). Only the winter of 2009–2010 had an anomaly under 10 K (7.3 K). Looking at the maximum temperature anomaly at 10 hPa, it is usually larger than 20 K, except during the winter of 2009–2010 (17 K). During the winters of 2007–2008, 2008–2009, 2015–2016, and 2018–2019, the anomaly was superior to 30 K. At this altitude, the maximum anomaly and the average anomaly are not strongly correlated ($R = 0.52$) because for some vents, the temperature can decrease very abruptly after the maximum is reached while for other events, the decrease happens a few days later thus influencing the average over 10 days, independently from the value of the maximum. This is why the winter of 2020–2021 had a low 10-day average

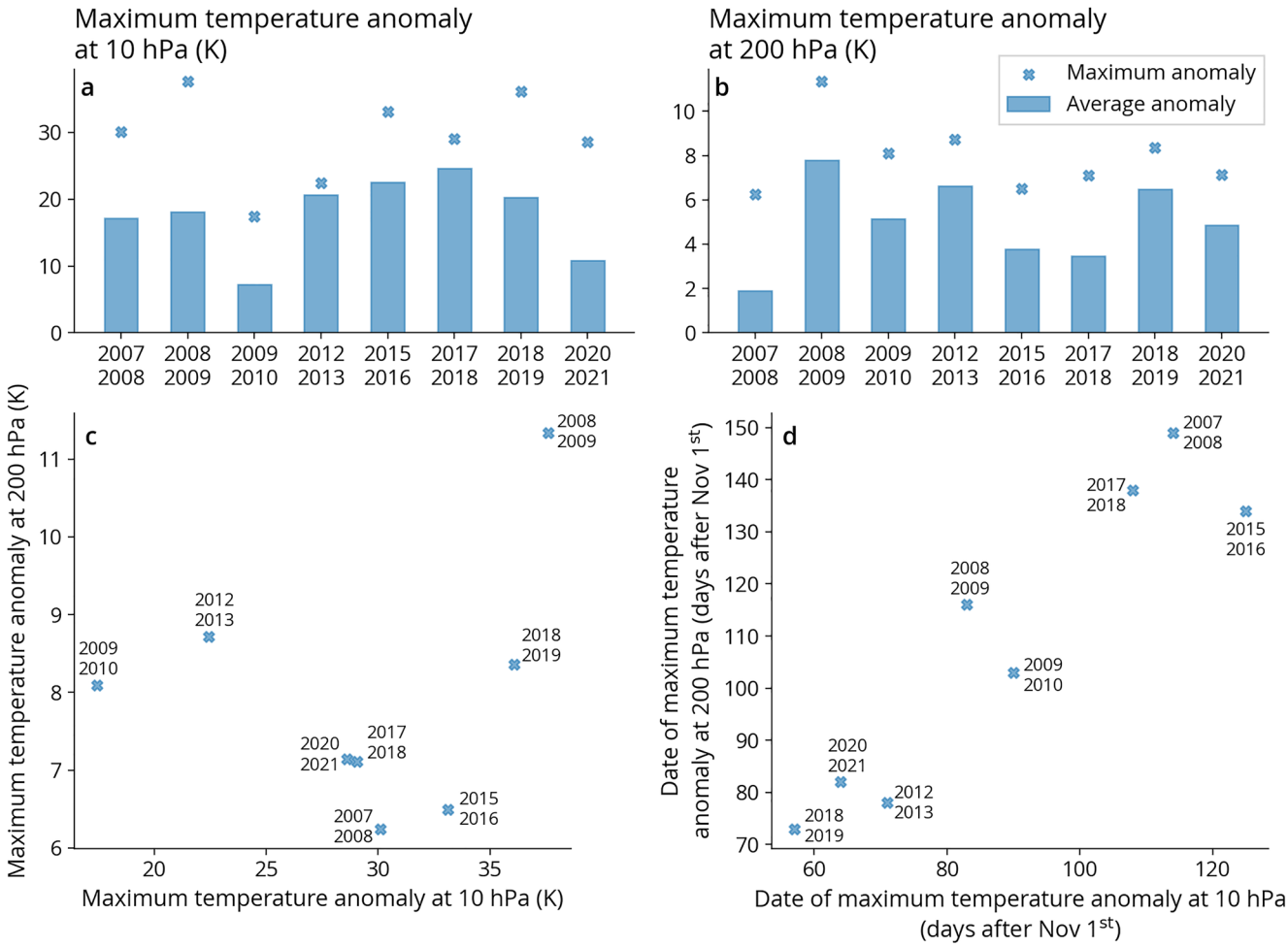

Figure 4. Maximum temperature anomaly at 10 hPa (a, crosses), average anomaly at 10 hPa in the 10 days following the zonal wind inversion (a, bars), maximum temperature anomaly at 200 hPa (b, crosses), average anomaly at 200 hPa in the 30 days following the zonal wind inversion (b, bars), relationship between the maximum temperature anomaly at 200 hPa and the maximum temperature at 10 hPa (c), relationship between the dates of the maximum anomaly at 200 and 10 hPa (d).

and a high maximum value. The winter of 2009–2010 had both a low average and a low maximum value that can be explained by the strong vortex at the beginning of the winter. This led to exceptionally cold conditions (Dörnbrack et al., 2012) that the SSW did not totally compensate, even though it was a strong event.

At 200 hPa (Figure 4b), the average anomaly in the 30 days following the zonal wind inversion is usually between 4 and 8 K, except during the winters of 2007–2008, 2015–2016, and 2017–2018 (1.9, 3.8, and 3.4 K, respectively). These low anomalies do not correspond to years with low anomalies at 10 hPa. The maximum anomalies are between 2 and 4 K larger than the average anomalies, except in 2007–2008 (difference of 4.3 K) and 2018–2019 (difference of 1.9 K), and the maximum and average anomalies are much more correlated than at 10 hPa ($R = 0.90$).

The relationship between the maximum anomalies at 200 and 10 hPa during major SSW winters is non-linear (Figure 4c), with the maximum anomaly at 200 hPa being between 6 and 9 K when the maximum anomaly at 10 hPa is between 15 and 30 K, and increasing from 6 to 11 K when the maximum anomaly at 10 hPa is superior to 30 K.

Figure 4d shows the relationship between the date at which the maximum anomalies at 200 and 10 hPa were reached, in days after November 1st. During major SSWs, when the maximum anomaly at 10 hPa is reached in late December-early January, the maximum anomaly at 200 hPa follows by one or two weeks (between 7 and 16 days after). However, when the maximum anomaly at 10 hPa is reached later in the winter, the maximum anomaly at 200 hPa can be more delayed: the maximum anomaly at 200 hPa can happen a month after the

maximum anomaly at 10 hPa, when the latter happen in late January or in February, as it was the case in March 2008, February 2009, and March 2018. For the years with minor SSWs (not shown here), the anomaly at 200 hPa (both the intensity and the date) is not related to the one at 200 hPa, as these events do not propagate to the lower stratosphere.

Note that as only eight major SSWs happened since the launch of the first IASI, these results would need to be consolidated in order to make robust conclusions.

3.2. Cold Waves at Mid Latitudes

Although SSWs happen in the polar stratosphere, they can strongly impact tropospheric winter weather at midlatitudes. The displacement or splitting of the polar vortex can cause positive temperature anomalies in Greenland, Northern Canada, Alaska and the Middle East and negative anomalies in Siberia, and Northern Europe in the month following the SSW (Butler et al., 2017; Davis et al., 2022; Kretschmer et al., 2018). They can also cause cold air outbreaks in the USA and Europe, such as the recent cold spells of February 2018 (Europe) and February 2021 (USA) that were caused by the major SSWs that occurred a few weeks before (Cohen et al., 2021; King et al., 2019).

Figure 5 shows the temperature anomaly at 750 hPa averaged over the 20 days following the zonal wind inversion for the eight major SSW winters, as well as the average anomaly for the eight winters. We chose to average the anomalies over a period of 20 days, instead of a whole month to show the anomalies before they start to significantly decrease: for a period of 30 days, the anomalies are very similar but slightly smaller.

We see that the anomalies vary over the different years. In Canada, we see a negative anomaly of 6 K in 2012–2013 and smaller anomalies between Eastern Canada and Greenland in 2007–2008 and 2018–2019. In 2017–2018, there was an anomaly of −4 K covering most of Canada and the west of the USA. The other winters show positive anomalies over this region, with strongest ones being in 2009–2010 (7 K) and 2020–2021 (6 K). These large positive anomalies are not necessarily linked to strong SSWs, as the maximum anomalies at 10 hPa were 17 and 29 K, respectively.

In Europe and Asia, there was a positive anomaly over both regions in 2007–2008 (2 K, 4 K in Western Russia). In 2015–2016, the anomalies were close to zero over all Eurasia. The other winters show negative anomalies over at least one of the two regions, most notably the winter of 2017–2018, with an anomaly of −3 K from Western Europe to Eastern Asia (with a maximum of −6 K in Europe) and the winter of 2009–2010, with an anomaly of −5 K circling almost the whole globe at around 50–60°N. The winters of 2007–2008 and 2018–2019 only showed small anomalies.

As surface temperatures are affected by several atmospheric phenomena other than SSWs, such as the Brewer-Dobson circulation, the Quasi-Biennial Oscillation or El Niño-Southern Oscillation, the surface temperature anomalies following the wind inversion vary significantly over the different years. However, SSWs are often associated with the negative phase of the North Atlantic Oscillation, leading to a persistent blocking over Greenland (Domeisen & Butler, 2020). Hence, when looking at the eight winter average, we find a more regular pattern, matching the previous studies: we see that SSWs are usually followed by a positive anomaly over Canada and Greenland (∼3 K over Canada and ∼6 K over Western Greenland) and in Southern Asia (∼2 K). We also see a negative anomaly over Europe and Northern Asia, that is largest over central Russia (−6 K).

In order to illustrate an example of cold air outbreak in the troposphere linked to SSWs, we show in Figure 6 the evolution of tropospheric temperature at 750 hPa in Europe in February 2018 and in the USA in February 2021. In February 2018, we see a mild negative anomaly (5 K) in most of Europe on the 21st and 22nd. After a few days, the anomaly increases as cold air from the east moves toward Western Europe. In the last three days of February, the anomaly reached −15 K in Western Europe, before dissipating in early March.

Over the USA in February 2021, we see a cold air mass from Canada starting to move South on February 4th. The intensity of the anomaly then increased as it moved further South and East, until it reached its maximum (−15 K) on the 7th and 8th of February. For both of these cold air outbreaks, we see that the negative anomaly comes from the regions where cold air from the vortex was moved to after the vortex split on Figure 2.

Figures S1 and S2 in Supporting Information S1 show the temperature anomalies at 750 hPa in Europe and North America after the eight zonal wind inversions (the dates are all within the month after the inversion but were

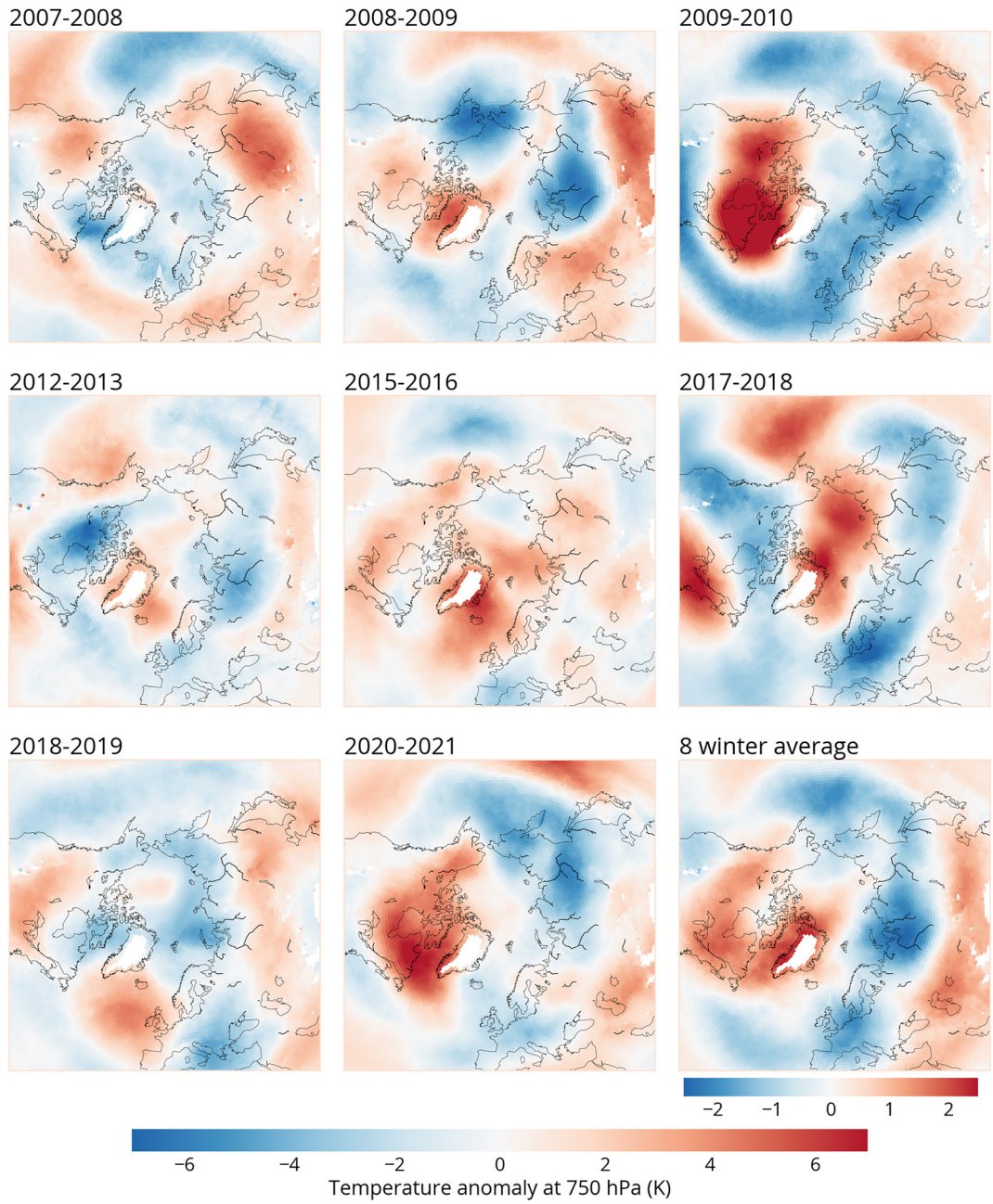

Figure 5. Temperature anomaly at 750 hPa averaged over the 20 days following the zonal wind inversion for the eight major SSWs and average of 8. Note that the color scale for the eight-winter average map is different than for single-winter maps.

chosen to show the cold air incursions). We see that cold outbreaks are very frequent after major SSWs, and they usually follow the same patterns: from North to South East in the USA, and from North East to South West in Europe. The most notable outbreaks occurred in March 2008, January 2009, January 2013, March 2016, and January 2019 in the USA and in February 2008, and March 2010 in Europe, although their effects did not always reach the surface.

3.3. Evolution of Ozone During Major SSWs

Ozone concentrations can be greatly affected by SSWs, as these events have a strong influence on stratospheric transport of trace gases. During SSWs, warm air is brought to the pole by the wave forcing, enhancing ozone

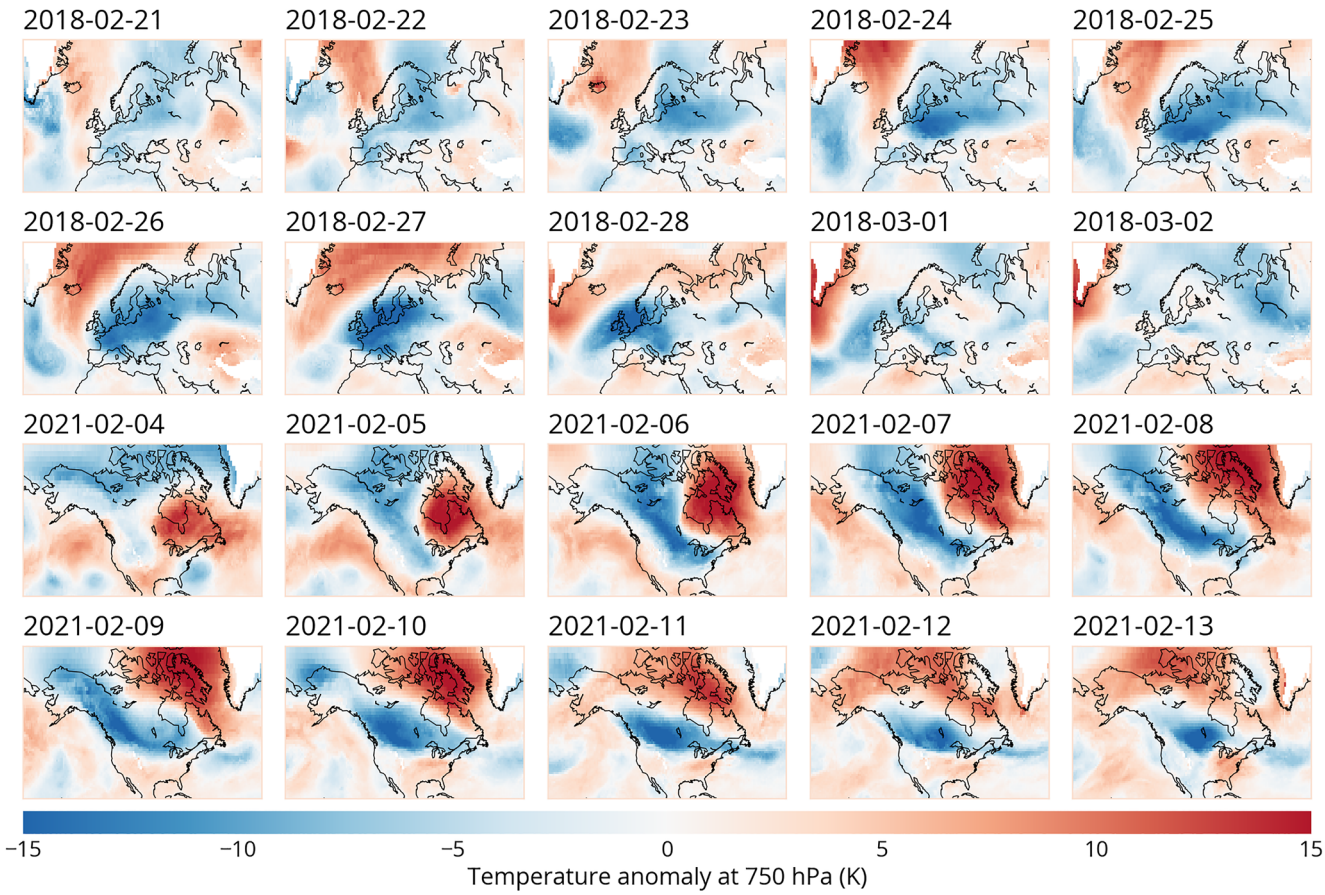

Figure 6. Temperature anomaly at 750 hPa in Europe in February 2018 (first two rows) and in North America in February 2021 (last two rows).

transport and mixing, and positive ozone anomalies are usually observed during these events (Bahramvash Shams et al., 2022). Furthermore, SSWs also affect the Brewer-Dobson circulation, with enhanced upwelling at the poles and downwelling in the tropics at the time of the event (De la Cámara, Abalos, & Hitchcock, 2018; Tao et al., 2017). As a result, polar ozone concentrations increase right after the vortex split or displacement. Figure 7 shows the evolution of the average total ozone column between 70°N and 90°N to represent ozone within the polar vortex during the eight major SSW winters (December to end of March) compared to the average of the 15 winters between 2007–2008 and 2021–2022.

During a typical seasonal distribution of polar ozone, the average ozone total column concentration increases steadily from December to March (WMO, 2018). During major SSWs, ozone concentrations are increasing, but with many days above the average. In 2007–2008, ozone started to increase around the 10th of January, at the same time as the first temperature gradient inversion (Table 1). It then decreased before increasing again in mid-February, when the major SSW happened (zonal wind inversion). This led to ozone concentrations being 50 DU larger than average in late February and mid-March. Similarly, in 2015–2016, ozone started increasing at the first temperature gradient inversion in late January-early February, before a stronger increase in early March (+180 DU in 20 days), with the inversion of zonal winds. As we see, on the figure, ozone concentrations were very low until mid-January, due to the record decrease in stratospheric temperatures (Manney & Lawrence, 2016). The several increases of temperature due to temperature gradient and zonal wind inversion prevented record ozone loss.

During the other winters with major SSWs, as the inversion of the temperature gradient and zonal winds happened nearly at the same time, there is usually only one strong increase of ozone. Ozone concentrations then stay above average for several weeks. Ozone concentrations stayed 20 DU above average during 50 days in 2008–2009, 2009–2010, 2012–2013, and in 2018–2019, where the positive ozone anomaly lasted the whole winter.

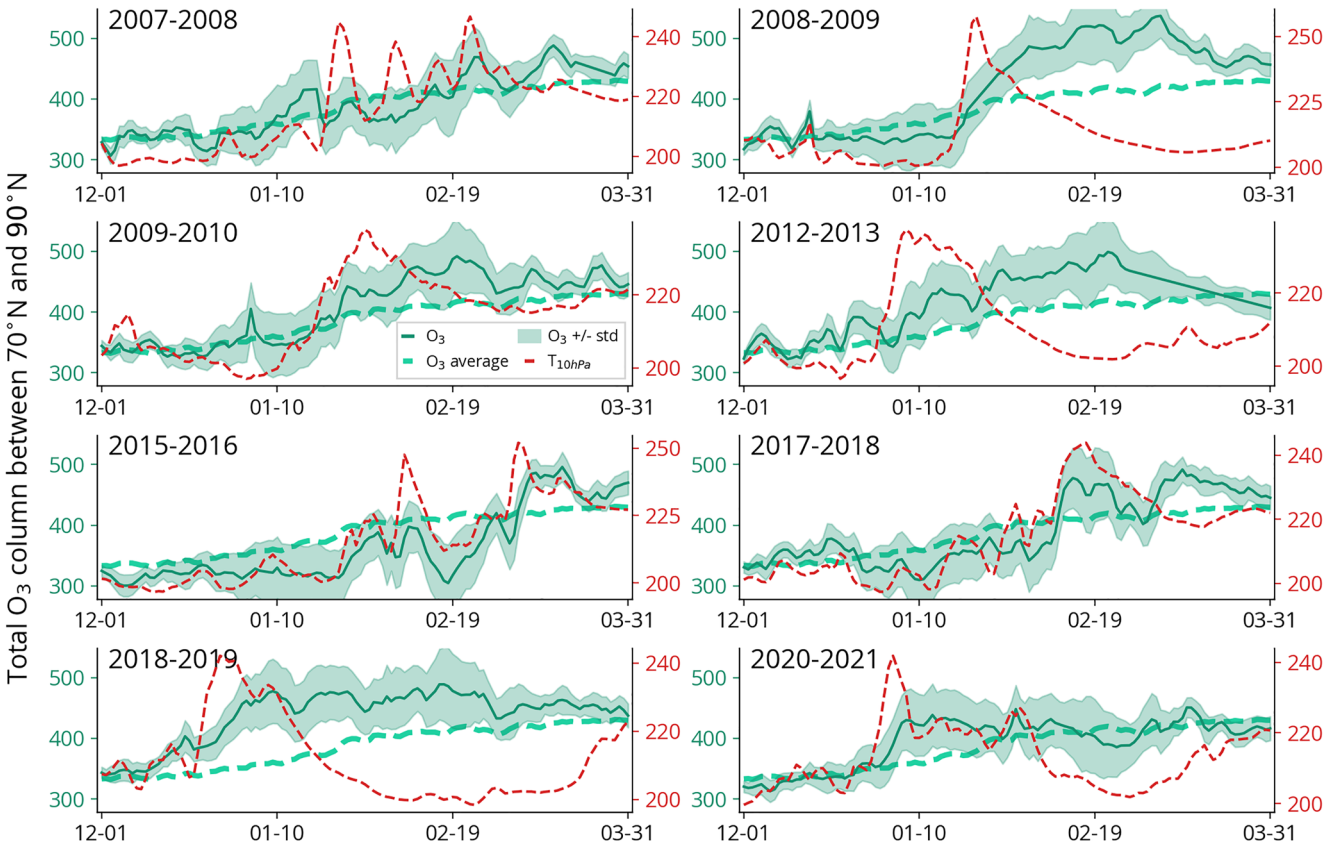

Figure 7. Daily average total ozone column during the eight major SSW winters (dark green, with the standard deviation shown around it) compared to average of all winters from 2007–2008 to 2020–2021 (dashed light green). The daily average temperature at 10 hPa is shown in red.

In addition to this, warm polar temperatures significantly hinder the ozone depletion process in spring: during a typical polar night, extremely cold temperatures allow the formation of polar stratospheric clouds (PSC) which contain ideal conditions for the creation of ozone depleting substances that are activated by the arrival of sunlight in spring. The warm stratospheric temperatures caused by SSWs partly prevent the formation of PSCs and ozone depleting substance, leading to higher ozone concentrations in the spring.

To study the effect of the SSWs on ozone depletion in spring, Figure 8a shows the maximum ozone anomaly observed during the eight winters with a major SSW, and the average anomaly in March alone. We see that the maximum anomaly is always between 60 and 80 DU, except in 2008–2009 and 2018–2019, where it reached 117.1 and 117 DU respectively. Most of the average anomalies in March are between 20 and 40 DU. March 2009 had a particurlay strong anomaly (61.2 DU), while March 2012–2013 had a low one (11.7 DU). The two largest anomalies observed (March 2009 and March 2018) can be due to the elongated shape of the polar vortex before the SSW (Bahramvash Shams et al., 2022). The year of 2020–2021, had a negative anomaly in March (−2.4 DU). This can be explained by the temperatures observed during this winter: the SSW happened early in the winter (zonal wind inversion on January 5th, see Table 1) and the temperature anomaly did not last very long in the stratosphere, it was almost completely dissipated in early February (see Figure 3), which left time for PSCs to form. The winter of 2012–2013 also had an zonal wind inversion in early February but, as we see on Figure 3, the temperature anomaly persisted until mid-February which impacted the ozone depletion process.

Figure 8b shows the relationship between the average ozone anomaly in March and the number of days during which the temperature anomaly between 10 and 200 hPa was larger than 5 K. We see that there is a general trend of the ozone anomaly increasing with the duration of the temperature anomaly, with the exception of March 2021, with an abnormally low ozone concentration due to the early date of the onset of the SSW, and March 2009, where ozone concentrations were exceptionally high. For the six other winters, the ozone anomaly increases from 10 DU when the temperature anomaly stays above 5 K for 30 days, to around 30 DU when the temperature

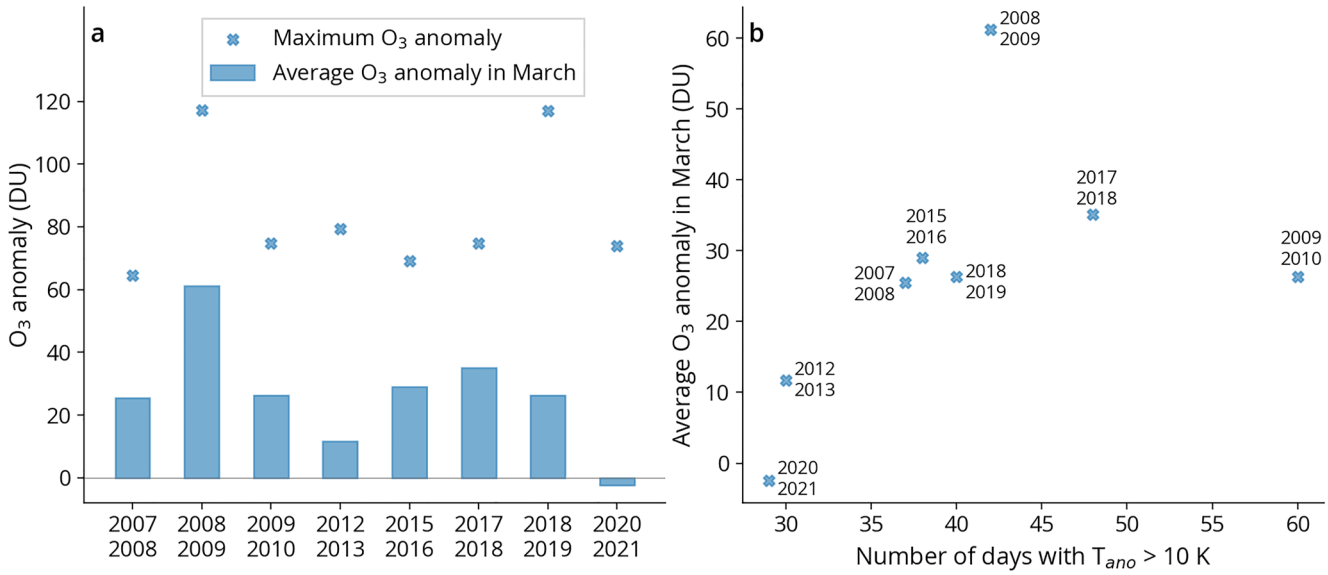

Figure 8. Maximum ozone anomaly and average anomaly in March (bars) (a), and relationship between the average anomaly in March and the number of days with a temperature anomaly between 10 and 200 hPa larger than 5 K (b).

anomaly stays above 5 K during 40 days or more, as the longer stratospheric temperatures stay above average the more PSC formation is impacted.

4. Conclusion

The IASI instruments have been monitoring atmospheric temperature and composition since 2007, allowing us to construct long and stable records of several atmospheric variables. IASI times series of atmospheric temperature and ozone concentrations are useful tools to study SSWs, as these two variables are the ones that are the most affected by SSWs. This study focuses on major SSW events, which have longer lasting effects and propagate lower into the stratosphere and in the troposphere. Four out of the eight major SSWs observed with IASI since 2007 were displacement events, and the others were split events. The maximum anomaly observed at 10 hPa ranges from 17 to 38 K, and they are not correlated to the type of event. Since the temperature anomaly propagates downwards to the tropopause during major SSWs, temperatures at 200 hPa increase significantly when the maximum anomaly at 10 hPa is larger than 30 K. Furthermore, the dates of the maximum anomaly at 200 hPa are linked to the dates of the anomaly at 10 hPa, as they are more delayed when the anomaly occurs later in the winter. IASI also monitors the temperature at 750 hPa, as SSWs are known to impact tropospheric weather at midlatitudes. We found that temperature anomalies vary over the different years, but on average there are positive anomalies over Canada and Greenland, and negative anomalies over Europe and Russia. We can also the cold air outbreaks that usually follow major SSWs in the USA and Europe.

SSWs also have a significant impact on polar ozone concentrations, as they disturb stratospheric dynamics and the formation of PSCs. Winters with major SSWs tend to have larger ozone concentrations in March than those without one. Most notably, average ozone concentrations in March are strongly correlated to the duration of the positive temperature anomaly at 10 hPa, except for the winters of 2010–2011 and 2019–2020 that had very low ozone concentrations due to very stable vortex conditions.

Some of the statistical results are not fully reliable, as they were only eight major SSWs since the beginning of the IASI mission. However, this shows the potential of the IASI instruments for the study of SSWs in the future, as they are planned to be operational until at least 2025, and they will be continued with the IASI-New Generation instruments until at least 2040 (Crevoisier et al., 2014). Furthermore, SSWs are also known to impact other trace gases, such as carbon monoxide, carbon dioxide or nitrous oxide (Jiang et al., 2013; Manney et al., 2009a, 2009b) and these gases can also be observed with IASI, SSW can be studied with collocated observations of these gases, in addition to ozone and temperature.

The evolution of SSWs in a changing climate is still unknown, as warm SSTs in the North Pacific are linked to a more stable vortex (Hu et al., 2018; Xia et al., 2021) but sea-ice loss is expected to weaken the vortex (Kim et al., 2014), and projections from models show different results (Kang & Tziperman, 2017; Mitchell et al., 2012). Hence the IASI and IASI-NG missions will help monitor and study the evolution of SSWs and their effects on ozone concentrations and tropospheric weather, as well as the connection of SSWs with climate change.

Data Availability Statement

ERA5 data can be downloaded from the Copernicus Climate Change Service Climate Data Store (Copernicus, 2018). The temperatures retrieved with the ANN can be downloaded on the IASI-FT website (Bouillon, 2021). IASI ozone data can be accessed from the Aeris website (Aeris, 2022).

Acknowledgments
This project has received funding from the European Research Council (ERC) under the European Union's Horizon 2020 and innovation program (Grant 742909, IASI-FT advanced ERC grant). The authors acknowledge the Aeris data infrastructure (https://www.aeris-data.fr/) for providing access to the IASI Level 1C data and Level 2 temperature data used in this study. The authors thank EUMETSAT through the Satellite Application Facility on Atmospheric Composition Monitoring (ACSAF) for the distribution of the IASI-ozone product.

References

Aeris (2022). The IASI O3 products processed with FORLI-O3 [Dataset]. IASI. http://iasi.aeris-data.fr/O3/

Bahramvash Shams, S., Walden, V. P., Hannigan, J. W., Randel, W. J., Petropavlovskikh, I. V., Butler, A. H., & de la Cámara, A. (2022). Analyzing ozone variations and uncertainties at high latitudes during sudden stratospheric warming events using MERRA-2. *Atmospheric Chemistry and Physics*, *22*(8), 5435–5458. https://doi.org/10.5194/acp-22-5435-2022

Baldwin, M. P., Ayarzagüena, B., Birner, T., Butchart, N., Butler, A. H., CharltonPerez, A. J., et al. (2021). Sudden stratospheric warmings. *Reviews of Geophysics*, *59*(1), e2020RG00070. https://doi.org/10.1029/2020RG000708

Baldwin, M. P., & Dunkerton, T. J. (2001). Stratospheric harbingers of anomalous weather regimes. *Science*, *294*(5542), 581–584. https://doi.org/10.1126/science.1063315

Bouillon, M. (2021). IASI-FT atmospheric temperature profiles [Dataset]. LATMOS/ULB. https://iasi-ft.eu/data-access/ATP/

Bouillon, M., Safieddine, S., Whitburn, S., Clarisse, L., Aires, F., Pellet, V., et al. (2022). Time evolution of temperature profiles retrieved from 13 years of infrared atmospheric sounding interferometer (IASI) data using an artificial neural network. *Atmospheric Measurement Techniques*, *15*(6), 1779–1793. https://doi.org/10.5194/amt-15-1779-2022

Boynard, A., Clerbaux, C., Coheur, P.-F., Hurtmans, D., Turquety, S., George, M., et al. (2009). Measurements of total and tropospheric ozone from the IASI instrument: Comparison with satellite and ozonesonde observations. *Atmospheric Chemistry and Physics*, *9*(16), 6255–6271. https://doi.org/10.5194/acp-9-6255-2009

Boynard, A., Hurtmans, D., Garane, K., Goutail, F., Hadji-Lazaro, J., Koukouli, M. E., et al. (2018). Validation of the IASI FORLI/Eumetsat ozone products using satellite (GOME-2), ground-based (Brewer-Dobson, SAOZ) and ozonesonde measurements. *Atmospheric Measurement Techniques*, *11*, 5125–5152. https://doi.org/10.5194/amt-2017-461

Boynard, A., Hurtmans, D., Koukouli, M. E., Goutail, F., Bureau, J., Safieddine, S., et al. (2016). Seven years of IASI ozone retrievals from FORLI: Validation with independent total column and vertical profile measurements. *Atmospheric Measurement Techniques*, *9*, 4327–4353. https://doi.org/10.5194/amt-9-4327-2016

Butler, A. H., Seidel, D. J., Hardiman, S. C., Butchart, N., Birner, T., & Match, A. (2015). Defining sudden stratospheric warmings. *Bulletin of the American Meteorological Society*, *96*(11), 1913–1928. https://doi.org/10.1175/BAMS-D-13-00173.1

Butler, A. H., Sjoberg, J. P., Seidel, D. J., & Rosenlof, K. H. (2017). A sudden stratospheric warming compendium. *Earth System Science Data*, *9*(1), 63–76. https://doi.org/10.5194/essd-9-63-2017

Charlton, A. J., & Polvani, L. M. (2007). A new look at stratospheric sudden warmings. Part I: Climatology and modeling benchmarks. *Journal of Climate*, *20*(3), 449–469. https://doi.org/10.1175/JCLI3996.1

Clarisse, L., R'Honi, Y., Coheur, P.-F., Hurtmans, D., & Clerbaux, C. (2011). Thermal infrared nadir observations of 24 atmospheric gases. *Geophysical Research Letters*, *38*, L10802. https://doi.org/10.1029/2011GL047271

Clerbaux, C., Boynard, A., Clarisse, L., George, M., Hadji-Lazaro, J., Herbin, H., et al. (2009). Monitoring of atmospheric composition using the thermal infrared IASI/MetOp sounder. *Atmospheric Chemistry and Physics*, *9*(16), 6041–6054. https://doi.org/10.5194/acp-9-6041-2009

Cohen, J., Agel, L., Barlow, M., Garfinkel, C. I., & White, I. (2021). Linking Arctic variability and change with extreme winter weather in the United States. *Science*, *373*(6559), 1116–1121. https://doi.org/10.1126/science.abi9167

Copernicus (2018). ERA5 hourly data on pressure levels from 1979 to present, Copernicus [Dataset]. CDS. https://cds.climate.copernicus.eu/cdsapp#!/dataset/reanalysis-era5-pressure-levels?tab=overview

Crevoisier, C., Clerbaux, C., Guidard, V., Phulpin, T., Armante, R., Barret, B., et al. (2014). Towards IASI-New Generation (IASI-NG): Impact of improved spectral resolution and radiometric noise on the retrieval of thermodynamic, chemistry and climate variables. *Atmospheric Measurement Techniques*, *7*(12), 4367–4385. https://doi.org/10.5194/amt-7-4367-2014

Davis, N. A., Richter, J. H., Glanville, A. A., Edwards, J., & LaJoie, E. (2022). Limited surface impacts of the January 2021 sudden stratospheric warming. *Nature Communications*, *13*(1), 1136. https://doi.org/10.1038/s41467-022-28836-1

De la Cámara, A., Abalos, M., & Hitchcock, P. (2018). Changes in stratospheric transport and mixing during sudden stratospheric warmings. *Journal of Geophysical Research: Atmospheres*, *123*(7), 3356–3373. https://doi.org/10.1002/2017JD028007

De la Cámara, A., Abalos, M., Hitchcock, P., Calvo, N., & Garcia, R. R. (2018). Response of Arctic ozone to sudden stratospheric warmings. *Atmospheric Measurement Techniques*, *18*(22), 16499–16513. https://doi.org/10.5194/acp-18-16499-2018

Domeisen, D. I. V., & Butler, A. H. (2020). Stratospheric drivers of extreme events at the Earth's surface. *Communications Earth & Environment*, *1*, 59. https://doi.org/10.1038/s43247-020-00060-z

Dörnbrack, A., Pitts, M. C., Poole, L. R., Orsolini, Y. J., Nishii, K., & Nakamura, H. (2012). The 2009–2010 Arctic stratospheric winter – General evolution, mountain waves and predictability of an operational weather forecast model. *Atmospheric Chemistry and Physics*, *12*(8), 3659–3675. https://doi.org/10.5194/acp-12-3659-2012

EUMETSAT (2018). IASI Level 1C climate data record release 1 - Metop-A [Dataset]. European Organisation for the Exploitation of Meteorological Satellites. https://doi.org/10.15770/EUM_SEC_CLM_0014

Hersbach, H., Bell, B., Berrisford, P., Hirahara, S., Horányi, A., Muñoz-Sabater, J., et al. (2020). The ERA5 global reanalysis. *Quarterly Journal of the Royal Meteorological Society*, *146*(730), 1999–2049. https://doi.org/10.1002/qj.3803

Hitchcock, P., & Simpson, I. R. (2014). The downward influence of stratospheric sudden warmings. *Journal of the Atmospheric Sciences*, *71*(10), 3586–3876. https://doi.org/10.1175/JAS-D-14-0012.1

Hu, D., Guan, Z., Tian, W., & Red, R. (2018). Recent strengthening of the stratospheric Arctic vortex response to warming in the central North Pacific. *Nature Communications*, *9*(1), 1697. https://doi.org/10.1038/s41467-018-04138-3

Hurtmans, D., Coheur, P.-F., Wespes, C., Clarisse, L., Scharf, O., Clerbaux, C., et al. (2012). FORLI radiative transfer and retrieval code for IASI. *Journal of Quantitative Spectroscopy and Radiative Transfer*, *113*(11), 1391–1408. https://doi.org/10.1016/j.jqsrt.2012.02.036

Jiang, X., Wang, J., Olsen, E. T., Pagano, T., Chen, L. L., & Yung, Y. L. (2013). Influence of stratospheric sudden warming on AIRS midtropospheric CO_2. *Journal of the Atmospheric Sciences*, *70*(8), 2566–2573. https://doi.org/10.1175/JAS-D-13-064.1

Kang, W., & Tziperman, E. (2017). More frequent sudden stratospheric warming events due to enhanced MJO forcing expected in a warmer climate. *Journal of Climate*, *30*(21), 8727–8743. https://doi.org/10.1175/JCLI-D-17-0044.1

Kim, B. M., Son, S. W., Min, S. K., Jeong, J. H., Kim, S. J., Zhang, X., et al. (2014). Weakening of the stratospheric polar vortex by Arctic sea-ice loss. *Nature Communications*, *5*(1), 4646. https://doi.org/10.1038/ncomms5646

King, A. D., Butler, A. H., Jucker, M., Earl, N. O., & Rudeva, I. (2019). Observed relationships between sudden stratospheric warmings and European climate extremes. *Journal of Geophysical Research: Atmospheres*, *124*(24), 13943–13961. https://doi.org/10.1029/2019JD030480

Kretschmer, M., Coumou, D., Agel, L., Barlow, M., Tziperman, E., & Cohen, J. (2018). More-persistent weak stratospheric polar vortex states linked to cold extremes. *Bulletin of the American Meteorological Society*, *99*(1), 49–60. https://doi.org/10.1175/BAMS-D-16-0259.1

Lu, Q., Rao, J., Guo, D., Yu, M., & Yu, Y. (2021b). Downward propagation of sudden stratospheric warming signals and the local environment in the Beijing-Tianjin-Hebei region: A comparative study of the 2018 and 2019 winter cases. *Atmospheric Research*, *254*, 105514. https://doi.org/10.1016/j.atmosres.2021.105514

Lu, Q., Rao, J., Liang, Z., Guo, D., Luo, J., Liu, S., et al. (2021a). The sudden stratospheric warming in January 2021. *Environmental Research Letters*, *16*(8), 084029. https://doi.org/10.1088/1748-9326/ac12f4

Lu, Q., Rao, J., Shi, C., Guo, D., Fu, G., Wang, J., & Liang, Z. (2022). Possible influence of sudden stratospheric warmings on the atmospheric environment in the Beijing–Tianjin–Hebei region. *Atmospheric Chemistry and Physics*, *22*(19), 13087–13102. https://doi.org/10.5194/acp-22-13087-2022

Manney, G., Santee, M., Rex, M., Livesey, N. J., Pitts, M. C., Veefkind, P., et al. (2011). Unprecedented Arctic ozone loss in 2011. *Nature*, *478*(7370), 469–475. https://doi.org/10.1038/nature10556

Manney, G. L., Harwood, R. S., MacKenzie, I. A., Minschwaner, K., Allen, D. R., Santee, M. L., et al. (2009b). Satellite observations and modeling of transport in the upper troposphere through the lower mesosphere during the 2006 major stratospheric sudden warming. *Atmospheric Chemistry and Physics*, *9*(14), 4775–4795. https://doi.org/10.5194/acp-9-4775-2009

Manney, G. L., & Lawrence, Z. D. (2016). The major stratospheric final warming in 2016: Dispersal of vortex air and termination of Arctic chemical ozone loss. *Atmospheric Chemistry and Physics*, *16*(23), 15371–15396. https://doi.org/10.5194/acp-16-15371-2016

Manney, G. L., Schwartz, M. J., Krüger, K., Santee, M. L., Pawson, S., Lee, J. N., et al. (2009a). Aura microwave limb sounder observations of dynamics and transport during the record-breaking 2009 Arctic stratospheric major warming. *Geophysical Research Letters*, *36*(12), L12815. https://doi.org/10.1029/2009GL038586

Maury, P., Claud, C., Manzini, E., Hauchecorne, A., & Keckhut, P. (2016). Characteristics of stratospheric warming events during Northern winter. *Journal of Geophysical Research: Atmospheres*, *121*(10), 5368–5380. https://doi.org/10.1002/2015JD024226

Mitchell, D. M., Osprey, S. M., Gray, L. J., Butchart, N., Hardiman, S. C., Charlton-Perez, A. J., & Watson, P. (2012). The effect of climate change on the variability of the northern hemisphere stratospheric polar vortex. *Journal of the Atmospheric Sciences*, *69*(8), 2608–2618. https://doi.org/10.1175/JAS-D-12-021.1

Rao, J., Garfinkel, C. I., & White, I. P. (2020). Predicting the downward and surface influence of the February 2018 and January 2019 sudden stratospheric warming events in subseasonal to seasonal (S2S) models. *Journal of Geophysical Research: Atmospheres*, *125*(2), e2019JD031919. https://doi.org/10.1029/2019JD031919

Rao, J., Liu, S., & Chen, Y. (2021). Northern hemisphere sudden stratospheric warming and its downward impact in four Chinese CMIP6 models. *Advances in Atmospheric Sciences*, *38*(2), 187–202. https://doi.org/10.1007/s00376-020-0250-0

Safieddine, S., Bouillon, M., Paracho, A.-C., Jumelet, J., Tencé, F., Pazmino, A., et al. (2020). Antarctic ozone enhancement during the 2019 sudden stratospheric warming event. *Geophysical Research Letters*, *47*(14), e2020GL087810. https://doi.org/10.1029/2020GL087810

Safieddine, S., Parracho, A. C., George, M., Aires, F., Pellet, V., Clarisse, L., et al. (2020). Artificial neural networks to retrieve land and sea skin temperature from IASI. *Remote Sensing*, *12*(17), 2777. https://doi.org/10.3390/rs12172777

Salmi, S.-M., Verronen, P. T., Thölix, L., Kyrölä, E., Backman, L., Karpechko, A. Y., & Seppälä, A. (2011). Mesosphere-to-stratosphere descent of odd nitrogen in February–March 2009 after sudden stratospheric warming. *Atmospheric Chemistry and Physics*, *11*(10), 4645–4655. https://doi.org/10.5194/acp-11-4645-2011

Scannell, C., Hurtmans, D., Boynard, A., Hadji-Lazaro, J., George, M., Delcloo, A., et al. (2012). Antarctic ozone hole as observed by IASI/MetOp for 2008-2010. *Atmospheric Measurement Techniques*, *5*(1), 123–139. https://doi.org/10.5194/amt-5-123-2012

Schoeberl, M. R. (1978). Stratospheric warmings: Observations and theory. *Reviews of Geophysics and Space Physics*, *16*(4), 521–538. https://doi.org/10.1029/RG016i004p00521

Tao, M., Liu, Y., & Zhang, Y. (2017). Variations in Brewer-Dobson circulation during three sudden stratospheric warming major warming events in the 2000s. *Advances in Atmospheric Sciences*, *34*(12), 1415–1425. https://doi.org/10.1007/s00376-017-6321-1

Thompson, D. W. J., Baldwin, M. P., & Wallace, J. M. (2002). Stratospheric connection to Northern hemisphere wintertime: Implications for prediction. *Journal of Climate*, *15*(12), 1421–1428. https://doi.org/10.1175/1520-0442(2002)015<1421:SCTNHW>2.0.CO;2

Van Loon, H., Jenne, R. L., & Labitzke, K. (1973). Zonal harmonic standing waves. *Journal of Geophysical Research*, *78*(21), 4463–4471. https://doi.org/10.1029/JC078i021p04463

Wespes, C., Hurtmans, D., Emmons, L. K., Safieddine, S., Clerbaux, C., Edwards, D. P., & Coheur, P.-F. (2016). Ozone variability in the troposphere and the stratosphere from the first 6 years of IASI observations (2008–2013). *Atmospheric Chemistry and Physics*, *16*(9), 5721–5743. https://doi.org/10.5194/acp-16-5721-2016

WMO. (2018). Scientific assessment of ozone depletion: 2018. In *Global ozone research and monitoring project–report No. 58* (p. 588).

Xia, Y., Hu, Y., Zhang, J., Xie, F., & Tian, W. (2021). Record Arctic ozone loss in spring 2020 is likely caused by North Pacific warm sea surface temperature anomalies. *Advances in Atmospheric Sciences*, *38*(10), 1723–1736. https://doi.org/10.1007/s00376-021-0359-9